The optical analysis of the proposed Schmidt camera design.

M. Hrabovsky, M. Palatka , P. Schovanek

Joint Laboratory of Optics of Palacky University and Institute of Physics of the Academy of Sciences of the Czech Republic

J. Grygar, J. Ridky, L. Soukup

Institute of Physics of the Academy of Sciences of the Czech Republic

GAP - 99 - 025

Abstract

In this note we study optical properties of the proposed Schmidt system with and without a corrector plate. We focused our attention on the analysis of energy distribution in the light spot on the focal surface. We present three-dimensional results of the energy distributions in the case of the ideal mirror and for the system with 1 mRad imperfections.

1 Introduction

The proposed optical system is widely used because it is very simple and hence attractive. The Schmidt camera offers the unparalleled combination of a fast focal ratio with the large image angle. The lens-less camera is coma free and it has only a spherical aberration. The spherical aberration depends on the aperture and the focal length. The lens-less Schmidt system must have a small aperture in order to retain small aberrations. The focal ratios represent the effective limit of the speed of a Schmidt camera and at focal ratios faster than *f / 1.5* more complicated systems are usually used in telescope design applications. The proposed FD design is a very fast one. It has focal ratio *f / 1*. We have analyzed the image quality of proposed Schmidt camera with intention to compare our results with results published in previous GAP notes. We expected similar results but aim was to complete useful three-dimensional analysis.

Our motivation was also to show some differences in image quality of a lens-less Schmidt camera with and without internal obscuration by PMT camera body. The three-dimensional layout of the Schmidt system is shown in Fig. 1. We analyzed the system with following values of the parameters.

- Radius of curvature of the mirror R = 3 400 mm ,
- Diameter of the diaphragm D = 1700 mm,
- Field of view 30 x 30 degrees (20 degrees half field of view in the mirror corner),
- The size of the PMT camera body is 920 mm x 920 mm,

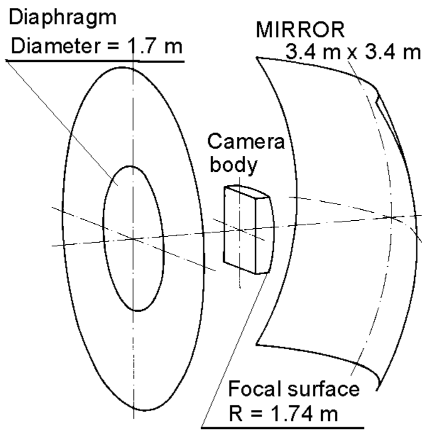

Figure 1: The lens-less Schmidt camera 3D scheme

The camera body obscures a central part of an incident bundle of rays. We used the circular obscuration with Diameter = 1200 mm for computation. The camera body has not rotational symmetry and it has diagonal dimension about 1300 mm. The diameter of a dummy surface D = 1200 mm is the approximation of the square shape which is rotated about the optical axis. The three-dimensional half drawing is shown in Fig. 2.

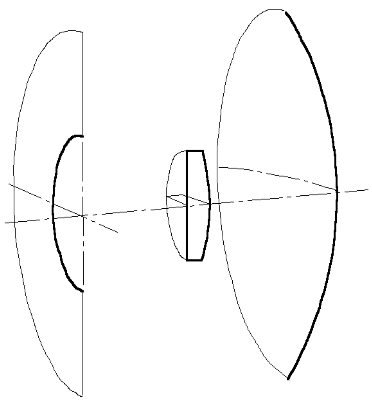

Figure 2: 3D drawing of the lens-less Schmidt camera used in computer analysis

2. The dependence of the spot structure on the obscuration

2.1 Spherical aberration and the disc of least confusion

Spherical aberration occurs when light rays parallel to the optical axis enter the system at different heights and come to the focus at different points along the axis of the lens-less Schmidt camera which has only the spherical aberration.
The following Fig. 3 shows the bundle of rays in the spherical mirror with focal ratio about *f/1*. We can see from this figure that the best image is shifted from paraxial focal plane.

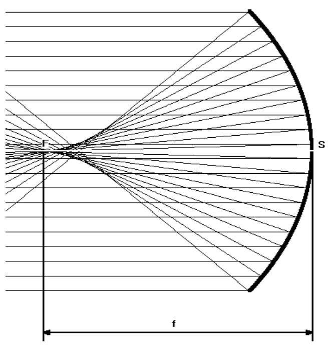

Figure 3: The spherical aberration of the mirror with the focal ratio *f / 1*.

The position of the best image plane is very important and we analyzed it like G. Matthiae and P. Privitera.

The rays near the paraxial focus point touch a surface of revolution called the caustic. The smallest image is where the ray from the rim of the pupil meets the caustic. The smallest image patch is called the disc of least confusion. The scheme is shown in the Fig. 4.

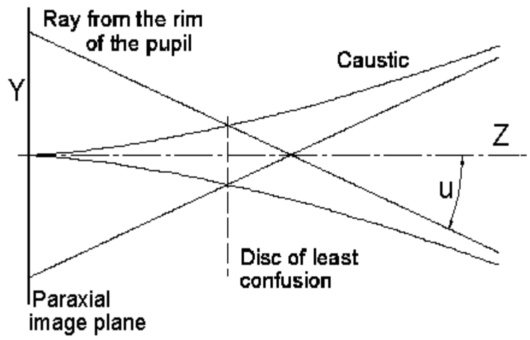

Figure 4: The scheme of the analysis of the smallest image patch.

The parametric equations of a ray reflected from the rim of the mirror are:

$$Y(t) = h + t \sin(u) \tag{1}$$

$$Z(t) = \Delta z + t \cos(u) \tag{2}$$

where h is the incident height of the ray ,
u is the angle of reflected ray ,
Δz is the height of the spherical cap

$$\Delta z = R \left(1 - \sqrt{1 - p^2}\right) \tag{3}$$

$$\cos(u) = 1 - 2p^2 \tag{5}$$

and $p = h / R$, where R is radius of curvature . It holds

$$\sin(u) = 2p \sqrt{1 - p^2} \tag{4}$$

The caustic is an envelope of reflected rays. Its parametric equations are

$$Y(p) = R\, p^3 \tag{6}$$

$$Z(p) = R\left(1 - \frac{1}{2}\sqrt{1 - p^2}\;\left(1 + p^2\right)\right). \tag{7}$$

Now we are able to find the intersection of ray from rim of the pupil and the caustic. We have found the disc of least confusion numerically. The exact location of the smallest image patch is shifted by 42.34 mm from the paraxial focal plane. The radius of curvature of PMT camera is then R = 1742.34 mm. It is in good agreement with result of G. Matthiae and P. Privitera. The diameter of the disc of least confusion is 14.83 mm. The Fig. 4 shows the envelope of the bundle of rays near the disc of least confusion. We have used another equation for reflected ray to draw this graph.

This equation is more informative than the parametric form,

$$Y(z) = z \tan(u) + \Delta y \tag{8}$$

where Δy is the transverse aberration,

$$\Delta y = LA \tan(u). \tag{9}$$

The longitudinal (spherical) aberration LA is:

$$LA = \frac{R}{2}\left(1 - \frac{1}{\sqrt{1-p^2}}\right) . \tag{10}$$

Since all the rays touch the caustic we might expect a great intensity of light in this region.
We have studied the intensity distribution at planes near the disc of least confusion.

2.2 The spot structure in the Schmidt camera with and without the obscuration

First we analyzed the intensity distribution at the best image plane and at three defocused planes with step 10 mm. The detailed view of the ray bundles near the focal plane in the camera without obscuration is shown in Fig. 5. The best image plane is shifted by 42.34 mm from the paraxial focal plane.
The second analysis concerned the camera with the internal obscuration of the diameter D = 1200 mm and its results can be compared with previous case. The detailed view is shown in Fig. 6. The figures have not the same magnification.

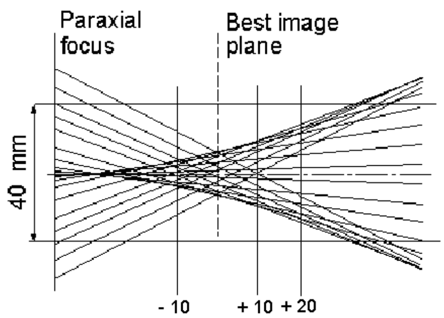

Figure 5: The ray bundles in the camera without the obscuration

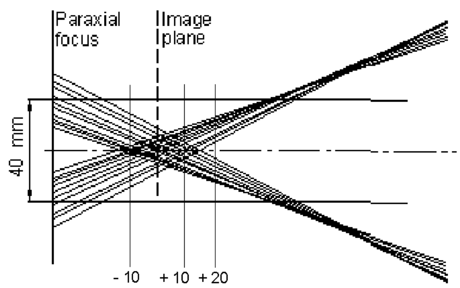

Figure 6: The ray bundles in the camera with the obscuration D = 1200 mm

We computed common spot diagrams of the system with and without obscuration before the analysis of the intensity distribution.
The spot diagrams were computed for fields of view 0, 10, 15, and 20 degrees respectively. The step was 5 mm between defocused planes. The following figures Fig. 7 and 8 show the spot structure and its deformation by the internal obscuration. The camera with internal obscuration has not uniform size and shape of the spot.

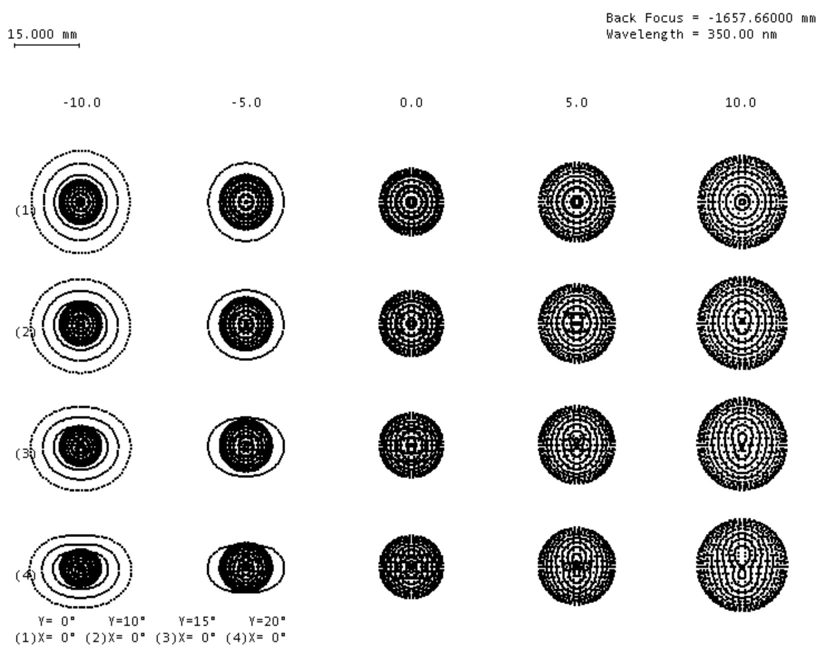

Figure 7: The spot diagrams of the lens-less Schmidt camera without internal obscuration

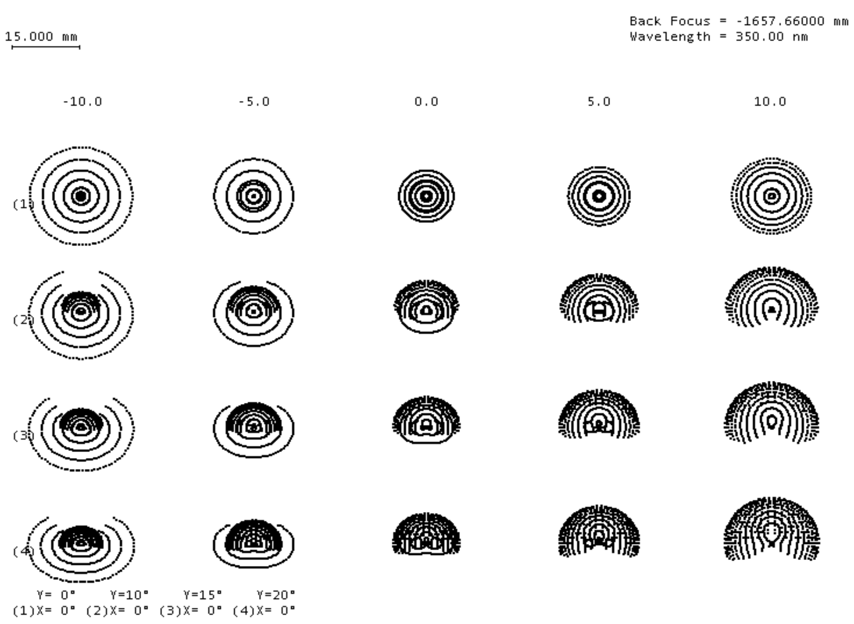

Figure 8: The spot diagrams of the lens-less Schmidt camera with the internal obscuration

The obtained pictures of the intensity distribution in light spots are similar to the those of radial distribution in GAP notes of G. Matthiae and P. Privitera and GAP notes of R.Sato, J.A.Belido C. and H.C.Reis [1, 2]
Our figures complete the information on spot structure in three dimensions.

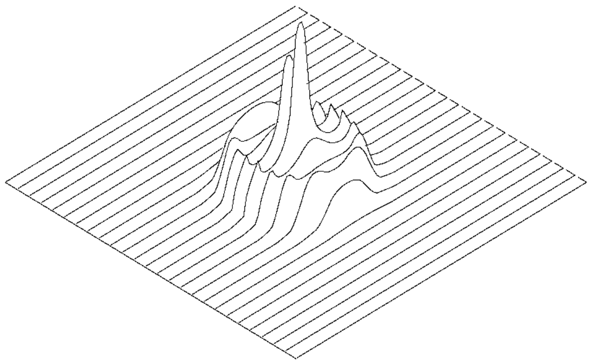

a ,

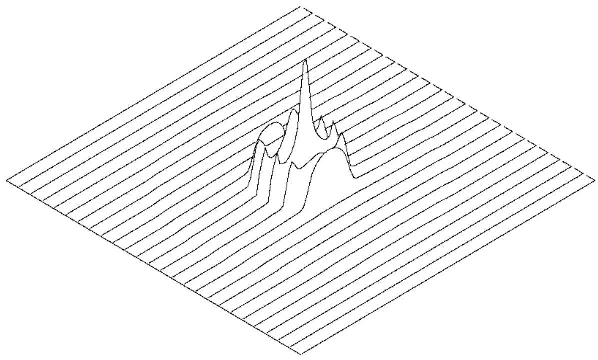

b ,

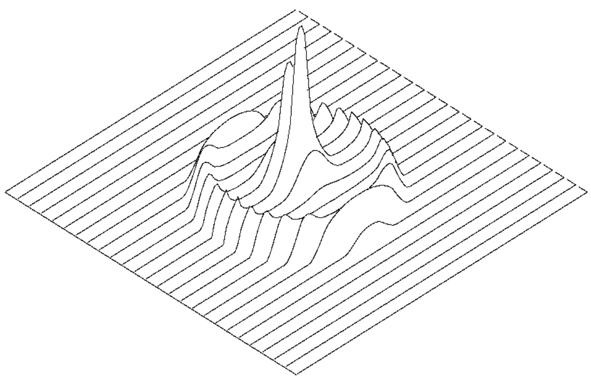

c ,

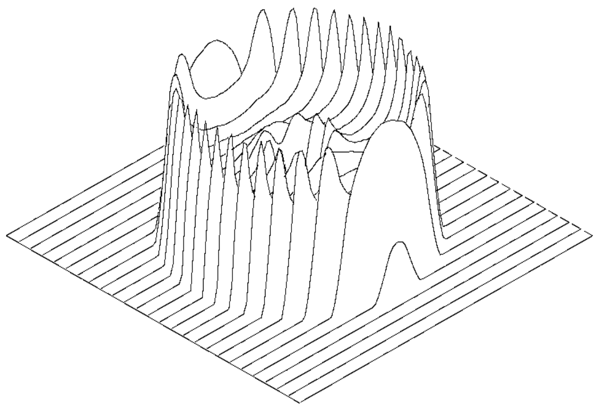

d,

Figure 9: The intensity distribution in the light spots for the lens-less Schmidt camera without internal obscuration for field of view 0 degrees.

a - the intensity distribution for the disc of least confusion,
b - image plane defocused by –10 mm (there is invisible circle of the edge light distribution),
c - image plane defocused by +10 mm,
d - image plane defocused by +20 mm.

The figures Fig. 9 a-d are in good agreement with typical ray intersection densities of spherical aberration as described in the optical engineering literature [3,4,5,6,7].
There is a high intensity peak in the center of the spot, which is rounded by a narrow ring at the disc of least confusion plane. The central peak will disappear when the image plane will be shifted towards the mirror but the shift must be more than 20 mm as shown in Fig. 9d.
The array dimensions in Fig. 9 are 40 mm x 40 mm.

The previous figure shows only the theoretic case of the camera because the Schmidt camera without the obscuration is not real but it is useful to know the image quality limit of the spherical mirror.
We have analyzed the intensity distribution for the Schmidt camera with the internal obscuration of the diameter D = 1200 mm. The Fig. 10 shows results at several image planes similarly as in the Fig. 9. We chose again the array with dimensions 40 mm x 40 mm. This area is comparable to the area of a PMT surface.

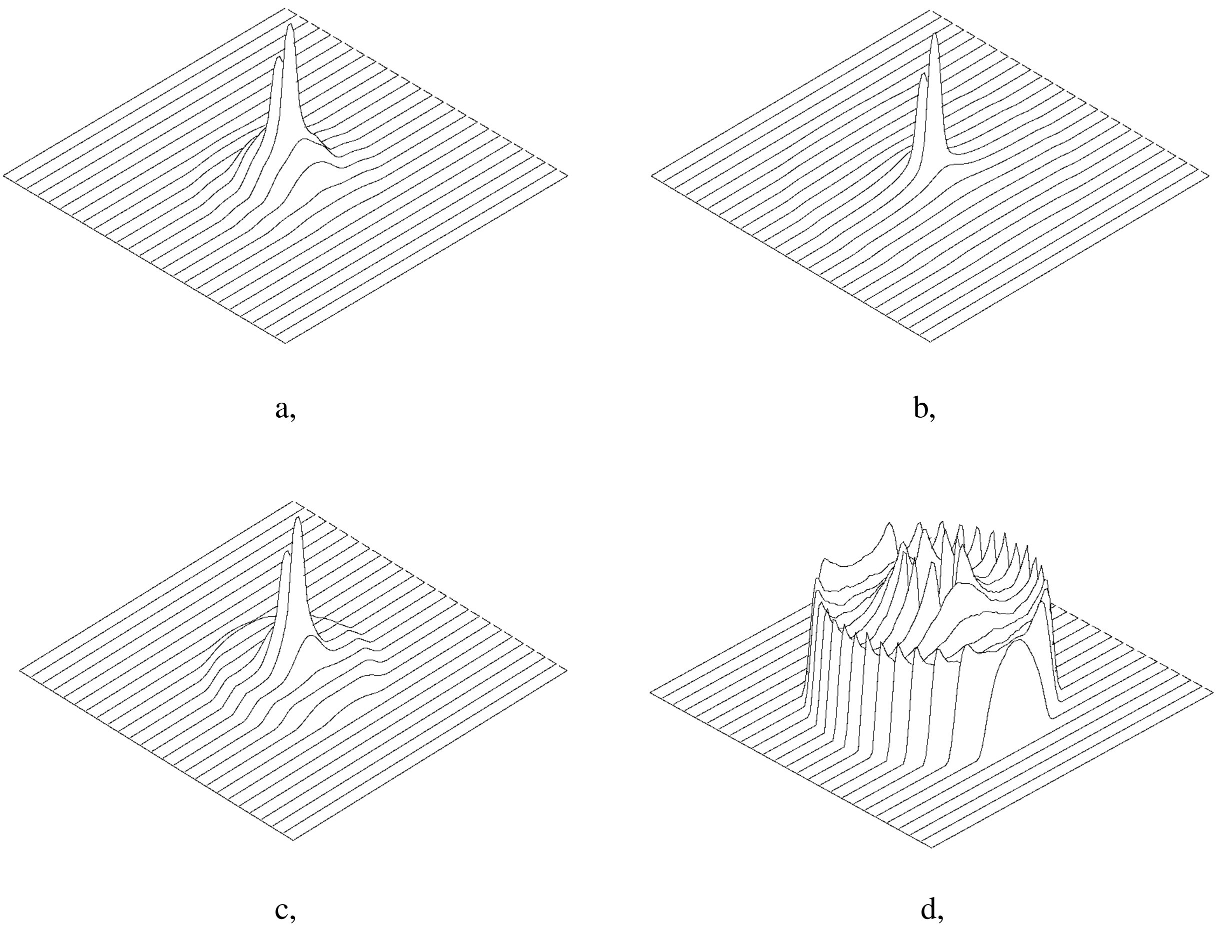

Figure 10: The intensity distribution in the light spots for the lens-less Schmidt camera with the internal obscuration (D = 1200 mm) for field of view 0 degrees.

a - the intensity distribution for the disc of least confusion,
b - image plane defocused by –10 mm (there is invisible circle of the edge light distribution),
c - image plane defocused by +10 mm,
d - image plane defocused by +20 mm.

The Fig. 10 shows one important difference compared to the camera without the internal obscuration. The internal obscuration stops part of the incident ray bundle. This causes the ring wall of the intensity distribution around the central peak.

The size and shape of the spot in Schmidt camera without internal obscuration are the same in the whole field of view in the interval from 0 degrees to 20 degrees. The spot is independent of the light arrival direction. The non-uniform spot shape appears when we use an internal obscuration. The following Fig. 11 shows the intensity distribution for the lens-less Schmidt camera with internal obscuration of the diameter D = 1200 mm and the field of view 20 degrees.

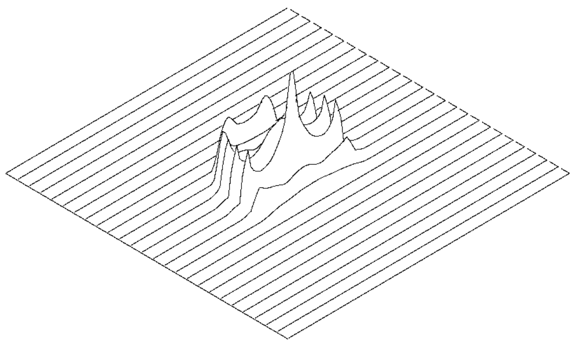

a,

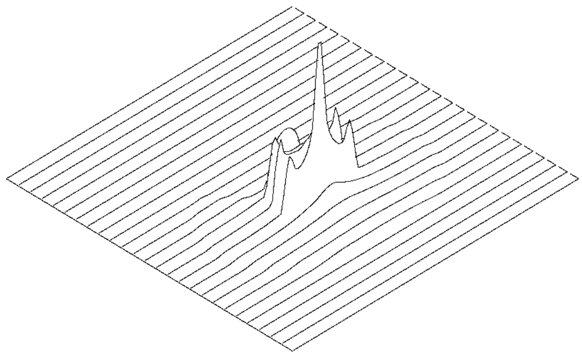

b,

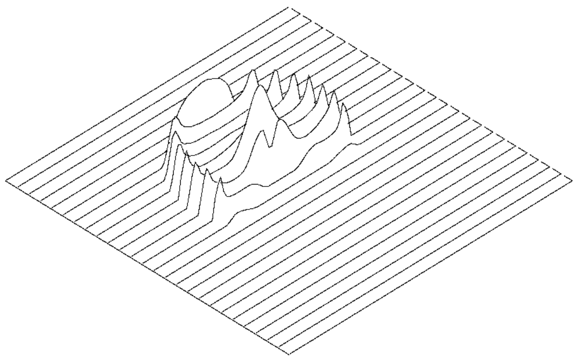

c,

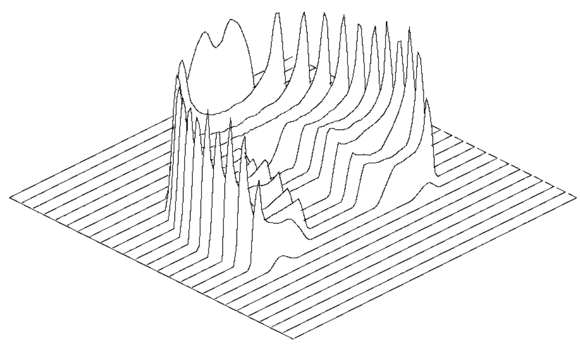

d,

Figure 11: The intensity distribution in the light spots for the lens-less Schmidt camera with the internal obscuration (D = 1200 mm) for field of view 20 degrees.

a - the intensity distribution for the disc of least confusion,
b - image plane defocused by –10 mm (there is invisible circle of the edge light distribution),
c - image plane defocused by +10 mm,
d - image plane defocused by +20 mm.

We can see the difference of the intensity distribution for the light spot in the case when the light arrival direction is changed from 0 degrees to 20 degrees. The ring of intensity around the central peak reappears again when the field of view is 20 degrees.

3. The classical Schmidt camera with the corrector plate.

The classical Schmidt camera has the corrector plate in the diaphragm to reduce the spherical aberration. We analyzed the optimal profile shape of the corrector plate like G. Matthiae and P. Privitera [1]. The profile shape must be chosen so that the optical path length from the entrance pupil to the focus is the same for all zones.
The profile satisfies the following equation

$$Z = A\,y^2 + B\,y^4 + C\,y^6 \qquad (11)$$

where Z is the depth of the curve,
y is the off-axis distance and
A, B, C are constants depending on the refractive index of the material, the focal ratio, the aperture and the position of the neutral zone.

For the focal ratios slower than *f / 3* the shape of the corrector plate may be described with sufficient accuracy by the two terms A and B only.
The equations in the textbook of Born and Wolf, *Principles of Optics,* use only two terms and these equations are found most often in the literature but they are only an approximation [8].
FD camera system has focal ratio about *f / 1* and hence we have taken also the third term C into account.

We found the constants A, B, C for the image plane shifted by 42.34 mm from the paraxial focal plane. This is plane of the disc of least confusion of the lens-less camera.
The Fig. 12 shows the drawing of the corrector plate with our results of the profile equation constants and the corrector plate specification.

Constants of the profile equations

$A = 1.3821447 \; 10^{-5}$

$B = -1.1044532 \; 10^{-11}$

$C = -1.7200000 \; 10^{-18}$

Material UV Acrylic
Diameter D = 1700 mm
Thickness = 15 mm
Max. depth = 3.97 mm

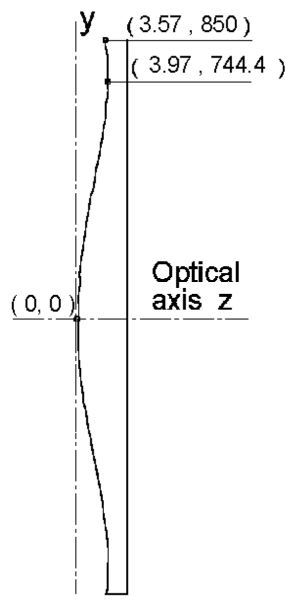

Figure 12: The corrector plate shape.

The corrector plate is a refracting element and it causes chromatic aberration. We analyzed the Schmidt camera with our design of corrector plate and the Fig. 13 and Fig. 14 show the spot diagrams for central wavelength 350 nm and for wavelength range 300 – 400 nm respectively.

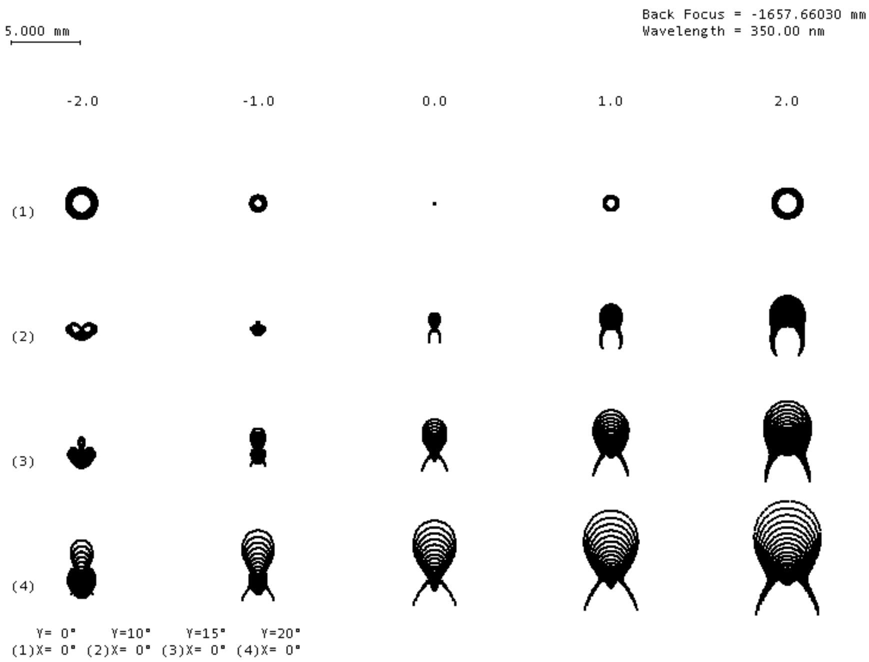

Figure 13: The spot diagrams of the Schmidt camera with the corrector plate (350 nm)

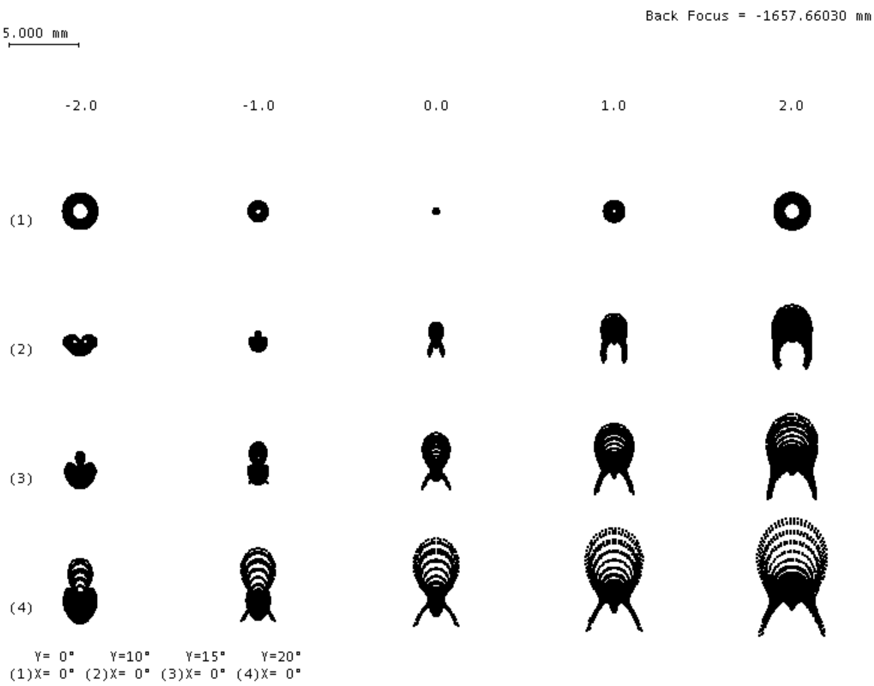

Figure 14: The spot diagrams of the Schmidt camera with the corrector plate (300 – 400 nm)

The spot diagrams were computed for fields of view 0, 10, 15, and 20 degrees respectively and the step was 2 mm between defocused planes. We can see from the spot diagrams that chromatic aberration is negligible in the chosen wavelength range 300 – 400 nm. The diameter of the spot is less than 0.1 mm in the case of 350 nm and it increases to 0.35 mm for the wavelength range 300 – 400 nm at best image plane and field of view 0 degrees. The diameter of light spot is about 0.08 mm for 0 degrees field of view but the corrector plate introduces some coma aberration. The maximal dimension of the spot is about 5 mm for the field of view 20 degrees. The spot size may be compensated for the whole field of view by shifting the corrector plate slightly towards the paraxial image plane.
We computed the intensity distribution in light spots for the Schmidt camera with the corrector plate for wavelength range 300 – 400 nm and some results are shown in Fig. 15.

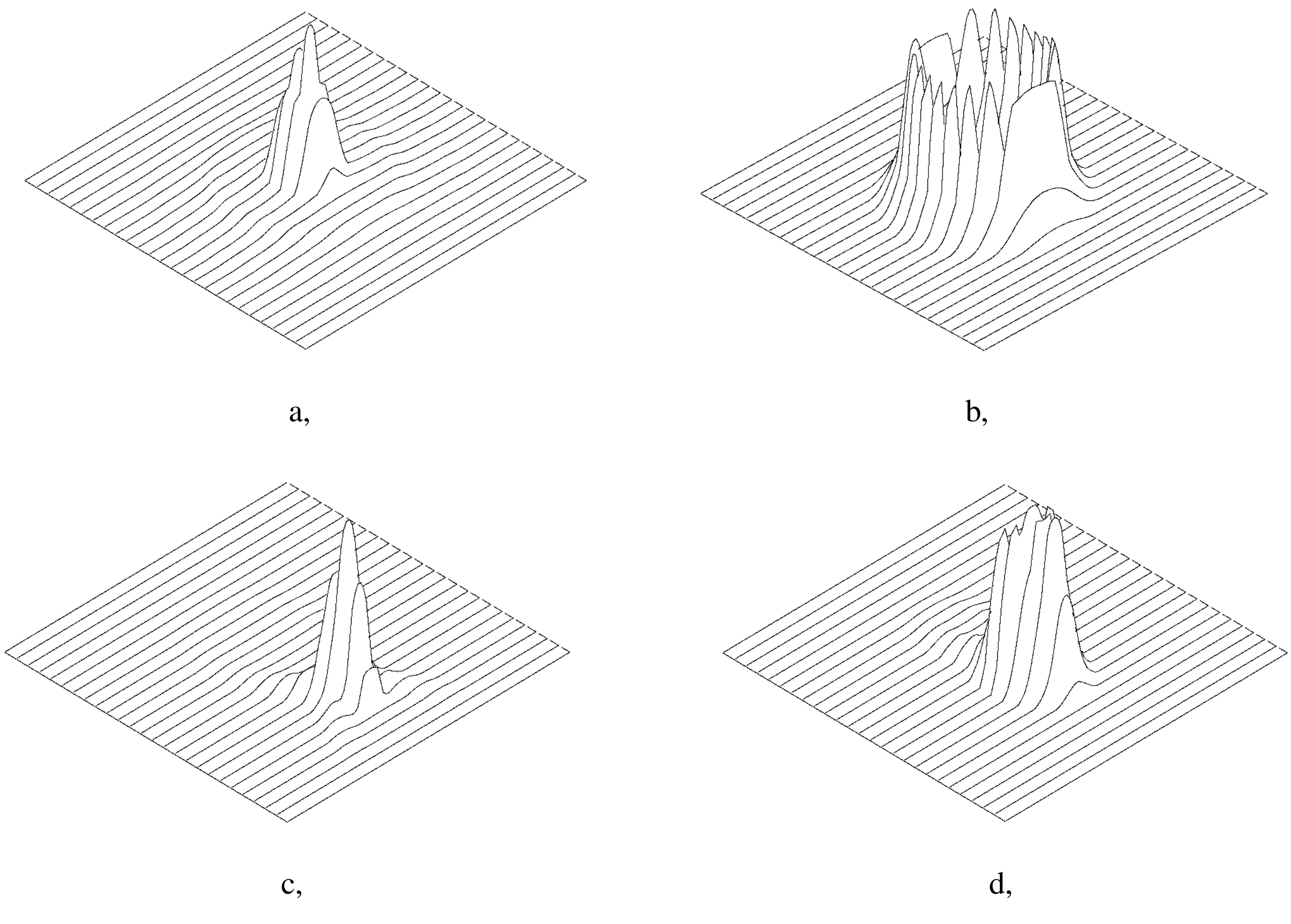

a, b, c, d,

Figure 15: The intensity distribution in the light spots for the Schmidt camera with the corrector plate for wavelength range 300 – 400 nm.

a - the intensity distribution for the disc of least confusion plane,
array dimensions are 0.5 mm x 0.5 mm, the field of view is 0 degrees
b - image plane is defocused – 2 mm ,
array dimensions are 5 mm x 5 mm, the field of view is 0 degrees
c - the intensity distribution at the disc of least confusion plane,
array dimensions are 5 mm x 5 mm, the field of view is 20 degrees
d - image plane is defocused - 2 mm,
array dimensions are 5 mm x 5 mm, the field of view is 20 degrees

4. The imperfection of the mirror surface

The previously presented results are valid for the perfect optical system. The introduction of some surface imperfection was the last step in our analysis. We simulated the surface slope error in range of 0 mRad - 1 mRad for the Schmidt camera with and without the corrector plate. We used the same weighting factors for all slope errors in the defined range. The following Fig. 16 and 17 show the intensity distribution.

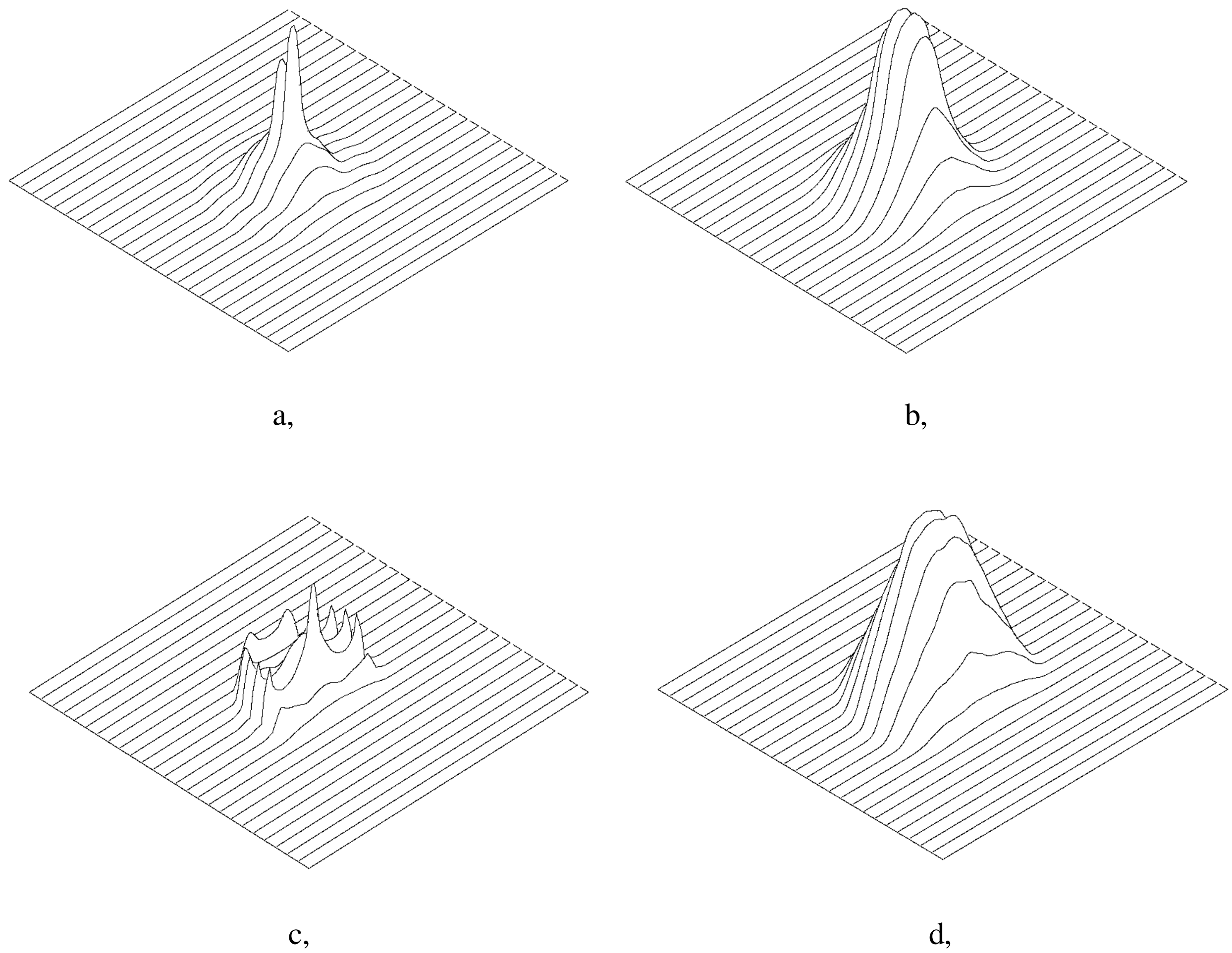

Figure 16: The intensity distribution in the light spots for the lens-less Schmidt camera with the internal obscuration D = 1200 mm and in the disc of least confusion plane. The array dimensions are 40 mm x 40 mm.

a - the intensity distribution for the field of view 0 degrees and no slope error,
b - the intensity distribution for the field of view 0 degrees and the slope error 0-1 mRad,
c - the intensity distribution for the field of view 20 degrees and no slope error,
d - the intensity distribution for the field of view 20 degrees and the slope error 0-1 mRad.

We can see how the surface imperfections spread the light spot and blur the fine light distribution structure of the perfect camera system.

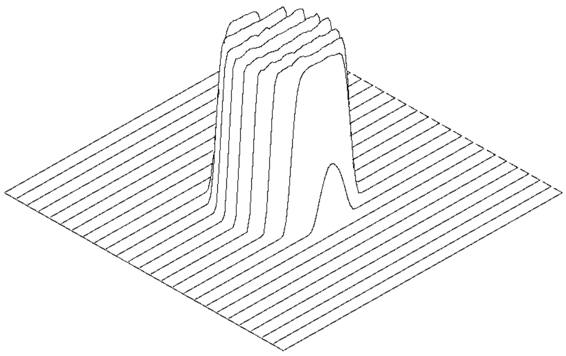

a,

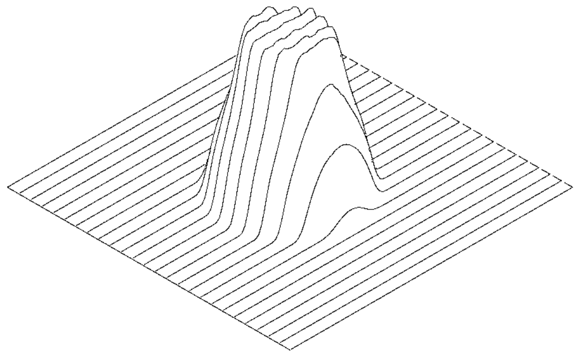

b,

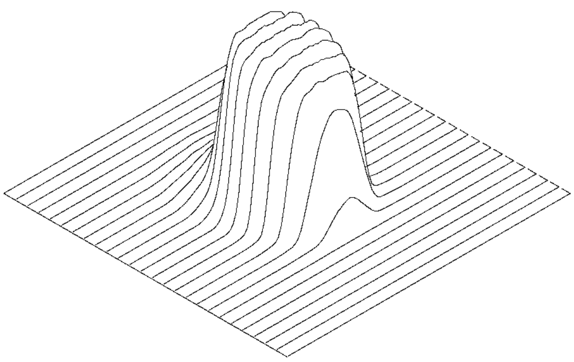

c,

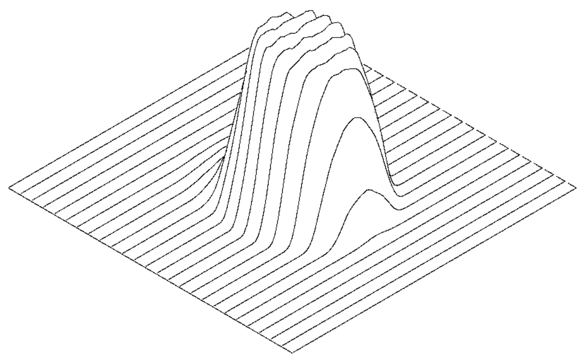

d,

Figure 17: The intensity distribution in the light spots for the Schmidt camera with the corrector plate for wavelength range 300 – 400 nm ,array dimensions are 20 mm x 20 mm, the slope surface error is in the range 0-1 mRad

a - the intensity distribution for the disc of least confusion plane, the field of view is 0 degrees
b - image plane is defocused – 2 mm, the field of view is 0 degrees
c - the intensity distribution at the disc of least confusion plane, the field of view is 20 degrees
d - image plane is defocused - 2 mm, the field of view is 20 degrees

We can compare the Fig. 15 with the Fig. 17 to see how the light spot is spread by the surface imperfections.

NOTE: The vertical scales of the intensities in cases a, b, c, d in some previous figures are not same due to limit of the image array resolution (100 x 100) used by program.

4. Conclusions

In this work we have analyzed the proposed camera system of FD. We found the exact position of the best image plane which leads to the radius of curvature of focal surface R = 1742.34 mm. The diameter of the disc of least confusion is D = 14.83 mm for the lens-less camera. We show the dependence of the intensity distribution in light spots on the defocusation and the internal obscuration.
We found the optimal profile of the corrector plate for reduction of the spherical aberration using the UV acrylic as suitable material for the wavelength range 300– 400 nm .
The use of the corrector plate increases the losses at the surfaces (about 8.4 %). The plate breaks the symmetry of camera system by coma aberration. The small shift of the focal plane can compensate the dimension of the light spot. We show the intensity distribution in spots.

Finally we have shown how the mirror surface imperfections blur the light spot structure and increase its dimension in case of lens-less camera and the camera with corrector plate.

Our analysis shows that only lens-less Schmidt camera without any internal obscuration produces the identical (shape and dimension) light spot in the whole field of view 0-20 degrees. When any internal obscuration is used, the shape of the spot made by oblique incident light has a cutout and no added optical element is able to make uniform the light spot in the whole field of view.
The proposed optical system is too fast and some non-uniformity of imaging will be always present.
We used our copy of the optical software SIGMA 2100 of KIDGER OPTICS [9] for the analysis.

References

[1] G. Matthiae and P.Privitera, Auger Technical Note, GAP/98/039

[2] R. Sato, J.A. Bellido C., H.C.Reis, Auger Technical Note, GAP/99/012

[3] W.T.Welford, Aberration of the Symmetrical Optical System, Academic Press, 1974

[4] H. Haferkorn, Optik, VEB Deutcher Verlag der Wissenschafen, Berlin , 1980

[5] H.Rutten and M.v.Venrooij, Telescope optics,Willman-Bell,Inc., 1989

[6] M.I.Apenko and A.C.Dubovik, Applied optics, Moscow, 1982, (in Russian)

[7] The Photonics Design & Applications Handbook, 1992

[8] M.Born and E.Wolf, Principles of Optics, Pergamon Press, 1980

[9] SIGMA 2100 optical design software, KIDGER OPTICS